UDK 669.058.67:519.876.5
Original scientific article/Izvirni znanstveni članek

ISSN 1580-2949
Mater. Tehnol.

NUMERICAL SIMULATION OF PARTICLE DEPOSITION EFFICIENCY IN HVOF SPRAYING : MATERIALS EFFECT

NUMERIČNA SIMULACIJA UČINKOVITOSTI NAPRŠEVANJA DELCEV NA PODLAGO PRI POSTOPKU TERMIČNEGA NAPRŠEVANJA Z VELIKO HITROSTJO; VPLIV MATERIALA

Rui Wang[1], Zunfei Xie[1], Xianghui Qi[1], Nianchu Wu[2]*

[1]School of Mechanical Engineering, Liaoning Petrochemical University, Fushun 113001, PR China
[2]School of New Energy and Advanced Materials, Liaoning Petrochemical University, Fushun 113001, PR China

Prejem rokopisa – received: 2025-10-27; sprejem za objavo – accepted for publication: 2026-01-22

doi:10.17222/mit.2025.1600

Particle critical velocity (for thermally sprayed particles) is not only the threshold for successful deposition of particles, but also a key parameter influencing deposition efficiency and coating quality. High velocity oxy-fuel (HVOF) thermal spraying is a well-established thermal spraying process, which has been extensively used in engineering fields. The coating produced by HVOF boasts the benefits of low porosity, low oxide content, and high adhesion. This study uses WC-Co and 316L stainless steel particles with different thermal conductivities as the spray particles, and develops the corresponding finite element models in Abaqus. A finite element model was developed to investigate two key aspects of HVOF thermal spraying: the relationship between particle critical velocity and particle diameter/temperature, and the influence of intrinsic material property variations on particle critical velocity. Numerical results show that particles with higher temperature and smaller diameter exhibit lower critical velocity and are more likely to form effective bonding with the substrate. Materials featuring high thermal conductivity and low specific heat capacity exhibit better heating capability. The better the heating ability, the more sensitive the material is. It can greatly affect the critical velocity, thereby enhancing the deposition efficiency of particles.

Keywords: HVOF, numerical simulation, critical velocity, deposition efficiency

Kritična hitrost delcev pri njihovem termičnem naprševanju na podlago ni le prag za uspešno naprševanje, temveč tudi ključni parameter, ki vpliva na učinkovitost nanašanja in kakovost prevleke. Termično naprševanje delcev z visoko hitrostjo v toku kisika in plinskega goriva (HVOF; High Velocity Oxy-Fuel thermal spraying) je uveljavljen postopek termičnega naprševanjanja, ki se pogosto uporablja na področju inženirstva za izdelavo trdih in/ali korozijsko odpornih prevlek. Prevleka, izdelana s HVOF postopkom ima mnoge prednosti, kot so majhna poroznost, nizka vsebnost oksidov in velika adhezija s podlago. V tem članku avtorji opisujejo HVOF postopek, pri katerem so uporabili delce nerjavnega jekla tipa 316L in delce WC-Co, ki imajo med seboj različno toplotno prevodnost. Na osnovi eksperimentalnih podatkov so nato avtorji izdelali ustrezne modele na osnovi končnih elementov s programskim orodjem Abaqus. Modeli na osnovi končnih elementov so bili izdelani za pomoč pri raziskovanju dveh ključnih vidikov termičnega naprševanja s HVOF postopkom: razmerja med kritično hitrostjo delcev in premerom ter kritično hitrostjo delcev in njihovo temperaturo ter vpliva sprememb notranjih (intrinsičnih) lastnosti materiala na kritično hitrost delcev. Numerični rezultati so pokazali, da imajo delci z višjo temperaturo in manjšim premerom nižjo kritično hitrost, in večjo verjetnost, da se bodo učinkovito vezali s podlago. Materiali z visoko toplotno prevodnostjo in nizko specifično toplotno kapaciteto pa kažejo boljšo sposobnost segrevanja. Boljša kot je sposobnost segrevanja, bolj občutljiv je material. Avtorji sklepajo, da bi to lahko močno vplivalo na kritično hitrost in s tem povečalo učinkovitost nanašanja delcev.

Ključne besede: termično naprševanje kovinskih delcev z visoko hitrostjo v toku plina (HVOF postopek), numerična simulacija, kritična hitrost, učinkovitost naprševanja

1 INTRODUCTION

High velocity oxy-fuel (HVOF) thermal spraying has replaced plasma spraying and become a mainstream technology in thermal spraying.[1,2] By producing coatings with excellent bond strength, higher density, and superior wear resistance, HVOF spraying has been widely utilized to improve wear resistance, corrosion resistance, and overall surface protection of componenets.[3–5] This improvement is primarily attributed to HVOF sprayed particles, which exhibit high impact velocity and low peak temperature. For HVOF coatings, a major practical challenge is achieving a deposition efficiency greater than 60 %. Given that the prices of WC-Co powders and other similar materials continue to rise, even a slight improvement in deposition efficiency may yield substantial economic benefits for the coating industry.[6] An increase in deposition efficiency means that more material can be deposited per unit, resulting in a more cost-effective process. Furthermore, deposition efficiency is directly related to the properties of the coating.[7] The increase in deposition efficiency directly determines both the economics of the process and the coating's properties (such as adhesion, density, and uniformity). Deposition efficiency is a critical parameter that affects productivity and manufacturing costs. The ability to predict deposition efficiency facilitates planning and budgeting, partic-

*Corresponding author's e-mail:
wunianchu@163.com (Nianchu Wu)

ularly for large-scale industrial applications.[8] Studies have shown that when the particle velocity surpasses the critical velocity, severe shear deformation and adiabatic shear instability promote the metallurgical bonding at the surface, between particle and the substrate. In contrast, the low velocity leads to particle rebound or inefficient deposition.[9]

Critical velocity is the threshold particle velocity at which particles can be deposited onto the substrate, and it is also a key parameter that affects deposition efficiency. Several factors influence critical velocity, including the physical properties of the thermal powder[10,11] and the corresponding process parameters.[12,13] Gu, Kamins et al.[14] reported that larger particles require higher critical velocities to achieve effective deposition. Within the simulated particle diameter range, 20–40 μm particles exhibit the highest deposition efficiency due to their optimal temperature and velocity. This makes them suitable for fabricating high-quality coatings. Jinxing Yu et al. analyzed the influence of the HVOF process on particle behavior (e.g., temperature, velocity, deposition efficiency) by combining computational fluid dynamics (CFD) simulation with experiments. The study demonstrated that by optimizing the key HVOF spraying process parameters, (e.g., spraying distance, oxygen-fuel ratio), it could balance low coating porosity, low residual stress, and high deposition efficiency. The research provides theoretical and practical guidance for making high performance coatings.[15] Bo Sun et al. could fabricate 316L stainless steel coatings with low oxidation and high compactness by using a new type of high-pressure HVOF system and adjusting the oxygen-fuel ratio as well as the spraying distance. With this method, the deposition efficiency can reach up to 90 %. They also discovered that when the spraying distance grows longer, deposition efficiency decreases.[16] Wolfgang Tillmann et al.[17–19] emphasized that particle velocity and temperature are the key factors determining the coating bonding strength. By optimizing the process parameters and spraying parameters, they influenced particle velocity and temperature. In HVOF thermal spraying, particle velocity and diameter are closely related to deposition efficiency. Notably, higher impact velocity reduces deposition efficiency, especially in the case of small particles. This is because finer particles are prone to erosion at high velocities. Within a reasonable range, higher temperature and velocity can improve the coating quality and enhance deposition efficiency.

In early studies, in order to find suitable spraying process parameters and clarify the relationship between these parameters and the final coating performance, experimental methods were used to investigate the HVOF spraying process. Although the results were highly reliable, the cost of the experiment is high, and the repeatability is poor. These methods could only measure the range of particle velocities rather than the velocity of individual particles.[20] However, with Hamid Assadi et al.[21] adopting numerical simulation to do particle impact experiments, the spraying process parameters including impact velocity, particle diameter, and temperature can be precisely controlled and adjusted in software. The simulation results can intuitively show the coatings. Thus, numerical simulation has gradually become a primary method. Furthermore, earlier research focused predominantly on the physical properties of particles and the process parameters of spraying systems. The effects of intrinsic particle properties (such as specific heat capacity and thermal conductivity) on deposition efficiency have been less studied. Thus, this study selects two types of particles with different intrinsic properties (WC-Co and 316L stainless steel) as the study objects. ABAQUS/Explicit software is used to simulate particle impact and analyze the coating deposition behavior.

Current research has gradually improved the prediction of critical velocity through theoretical modes and numerical simulations. However, the material differences, oxidation states, and multi-parameter coupling effects still remain challenges. The future research should further develop universal models and explore the correlation between microscopic bonding mechanisms and macroscopic properties, and promote the application of spraying technology in high-end fields. The objective of this paper is to explore the correlation between the critical velocity of particles, temperature, and diameter in the HVOF spraying process by using numerical simulation.

2 MODEL DEVELOPMENT

The finite element (FE) solver ABAQUS/Explicit is commonly employed to analyze solid impact dynamics, particularly in HVOF. The model includes a variety of factors, including thermal softening, strain hardening, and heating, being attributed to frictional and plastic dissipation. Since the particle diameter and time scale associated with the HVOF particle impact process are extremely small, heat transfer between the particle and substrate is effectively neglected. Consequently, the heating process is treated as adiabatic. The relevant material properties are presented in **Table 1**.

Table 1: Material properties of WC-Co and 316L stainless steel particles[6]

Material parameters	WC-Co	316L stainless steel
Density (kg/m^3)	14000	7890
Solidus temperature (K)	1580	1675
Solidus temperature (TS) (K)	1580	1675
Liquidus temperature (TL) (K)	1640	1708
Thermal conductivity (W/m·K)	36	16
Specific heat capacity (J/kg·K)	295	500
Young's modulus (GPa)	500	195
Poisson's ratio	0.27	0.3
Shear modulus (GPa)	197	75
Static shear strength, A (MPa)	1550	280
Strain-hardening modulus, B (MPa)	2200	1250

Strain rate sensitive coefficient, C	0.0312	0.07
Strain-hardening exponent, n	0.45	0.76
Thermal softening exponent, m	1.34	0.82
Reference temperature (K)	298	298
5432 Reference equivalent plastic strain rate (s^{-1})	1	1
Inelastic heat fraction	0.9	0.9
Speed of sound, C_0 (m/s)	3850	4600
$v_s - v_p$ slope	1.44	1.49
Gruneisen parameter	1.58	2.02

The linear elastic model describes the elastic response of materials, and this model can be used to study many impact scenarios.[6] The Johnson-Cook plasticity model is used to characterize the plastic response of WC-Co, and its details are provided as follows:

$$\sigma = (\varepsilon_p, \dot{\varepsilon}, T) = \left[A + B(\varepsilon_p)^n\right](1 + C \ln \dot{\varepsilon}^*)\left[1 - (T^*)^m\right] \quad (1)$$

In the model, A refers to the static shear strength, B denotes the strain-hardening modulus, C represents the strain rate sensitive coefficient, m stands for the thermal softening exponent, n is the strain-hardening exponent, ε_p is the equivalent plastic strain, $\dot{\varepsilon}^*$ and T^* are dimensionless variables. The definitions are as follows:

$$\dot{\varepsilon}^* = \frac{\dot{\varepsilon}}{\dot{\varepsilon}_0} \quad (2)$$

$$T^* = \frac{T - T_r}{T_m - T_r} \quad (3)$$

Here, $\dot{\varepsilon}$ denotes the equivalent plastic strain rate, $\dot{\varepsilon}_0$ is the reference equivalent plastic strain rate, T represents the material temperature, T_r stands for the material reference temperature, T_m is the melting temperature of the material, or the liquidus temperature. In addition, the MAT_JOHNSON_COOK material model requires an equation of state and uses the linear EOS_GRUNEISEN formulation. The equation for compressible materials is as follows:[22]

$$p = \frac{\rho c^2 \mu\left[1 + \left(1 + \frac{\gamma_0}{2}\right)\mu - \frac{a}{2}\mu^2\right]}{\left[1 - (S_1 - 1)\right]\mu - S_2\frac{\mu^2}{\mu+1} - S_3\frac{\mu^3}{(\mu+1)^2}} + (\gamma_0 + a\mu)E \quad (4)$$

Here, E denotes the internal energy per unit initial volume, c represents the v_s-v_p intercept of the curve, S_1, S_2 and S_3 stand for the slopes of the v_s-v_p curve, γ_0 is the Gruneisen parameter, and a is the first volume correction of γ_0, $\mu = \rho/\rho_0 - 1$.

A three-dimensional (3D) computational domain is used for the impact process, as illustrated in **Figure 1a**. Considering computational efficiency and cost, and given that the impact process between the particle and the substrate is axisymmetric, a quarter of the three-dimensional model is used for numerical simulation. The substrate diameter is set to ten times the particle diameter, and its height is seven times the particle diameter. Impact results can be observed more clearly with a larger model. In the finite element model (FEM), all directions of the substrate's bottom surface are constrained. The corresponding symmetric constraints are imposed on the quarter-symmetry plane of the particle and the substrate, while the other surfaces are left free. A surface-to-surface contact algorithm is adopted between the particle surface and the substrate surface. Mesh sensitivity analyses demonstrate that the mesh size is a major factor affecting material heating, subsequently affecting the shear flow localization.

In the numerical simulation of the WC-Co particle impact onto the 316L stainless steel substrate, the mesh size is approximately 1/30 of the particle diameter. Mapped meshing is adopted, a reduced-integration hexahedral element (C3D8RT) is used, and the number of mesh elements is 207,269. Due to the particles hitting the substrate, large deformation may occur during the impact process, which may lead to mesh distortion. This further affects computational accuracy or even terminates the computation. The advantages of the Arbitrary Lagrange-Euler (ALE) method include adaptive mesh-

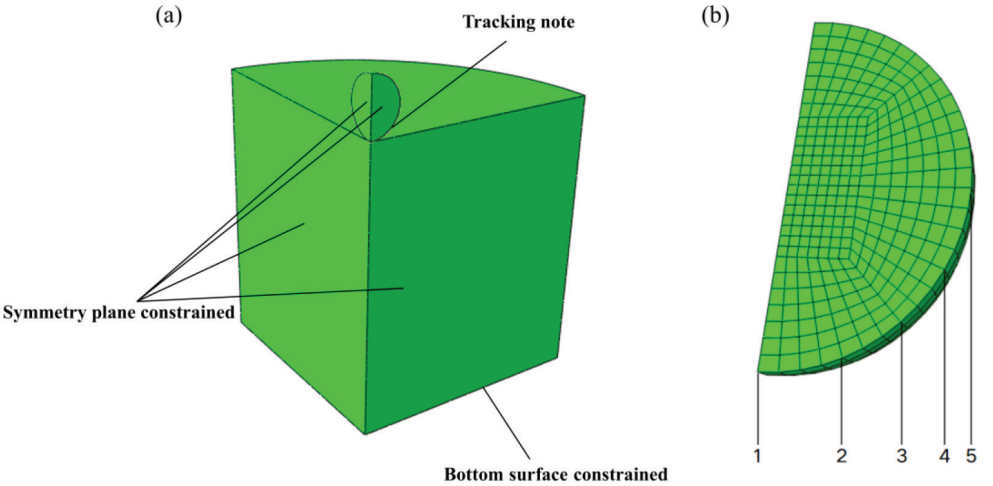

Figure 1: 3D finite element model in HVOF spraying: a) 3D domain of the impact process; b) tracking nodes

ing, enabling the mesh to move independently of the material, maintaining high-quality meshes. Thus, the ALE method is adopted to perform remeshing, thereby optimizing the computation. Furthermore, because first-order reduced-integration elements are used, it is necessary to apply hourglass control to prevent hourglass modes. It should be noted that in the ALE method, nodes do not move with the material; therefore, tracking nodal changes is meaningless. Thus, it is necessary to select tracking nodes on the impact particle's surface at the locations where severe plastic deformation may occur. The tracking nodes illustrated in **Figure 1b** are utilized to extract results related to the evolution maximum plastic strain, flow stress, and temperature over time.

3 RESULTS AND DISCUSSIONS

The simulation targets the impact of WC-Co particles and 316L stainless steel particles on 304 stainless steel substrates with a uniform temperature of 298 K. Due to variations in the particle diameter, impact velocity, and temperature, the simulation results show differences. This study focuses on WC-Co and 316L stainless steel particles, selects three particle diameters (20, 30, 40) μm, and aims to investigate variations in the critical velocity under different temperatures. When the particle diameter and temperature are constant, the effects of material property parameters on particles' critical velocity are analyzed.

3.1 Selection of tracking nodes and comparison of material heating capabilities

The evolution of the maximum plastic strain over time at various tracking nodes on WC-Co particles over time is presented in **Figure 2**. It shows that the tracking nodes at both ends of the path (i.e., Node 1 and Node 5) have the smallest variation amplitude in the maximum plastic strain. The closer to the middle of the path, the larger the variation amplitude. Node 3 has the largest variation amplitude. Therefore, Node 3 is selected as the tracking node to extract results related to the evolution of maximum plastic strain, flow stress, and temperature over time.

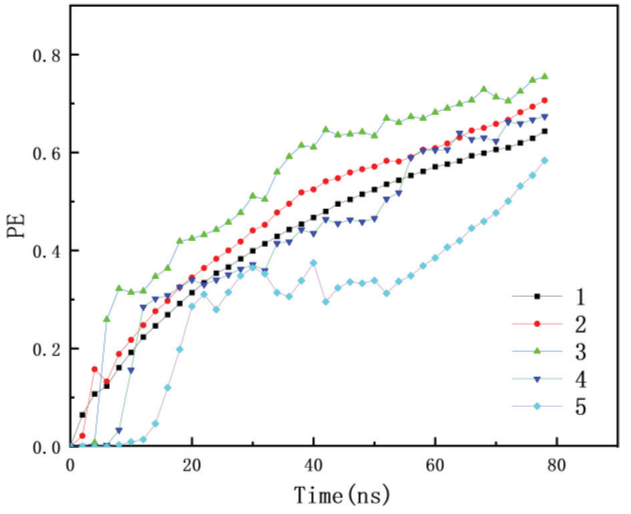

Figure 2: Maximum plastic strain of different tracking nodes

Simulations were conducted for WC-Co and 316L stainless steel particles with a diameter of 30 μm, and the results are shown in **Figure 3**. **Figure 3a** presents the simulation results for WC-Co particles with varying velocities at a temperature of 800 K, while **Figure 3b** presents the simulation results for the same particles with varying temperatures at a velocity of 300 m/s. **Figures 3b** and **3d** show the corresponding stress variation curves of WC-Co particles under changing velocity and temperature. The simulation results of 316L stainless steel are shown in **Figures 3e-3h**. Additionally, a comparative analysis of the performance of the two materials was also required. Under a temperature of 1100 K and a velocity of 500 m/s, the particle attains the melting tem-

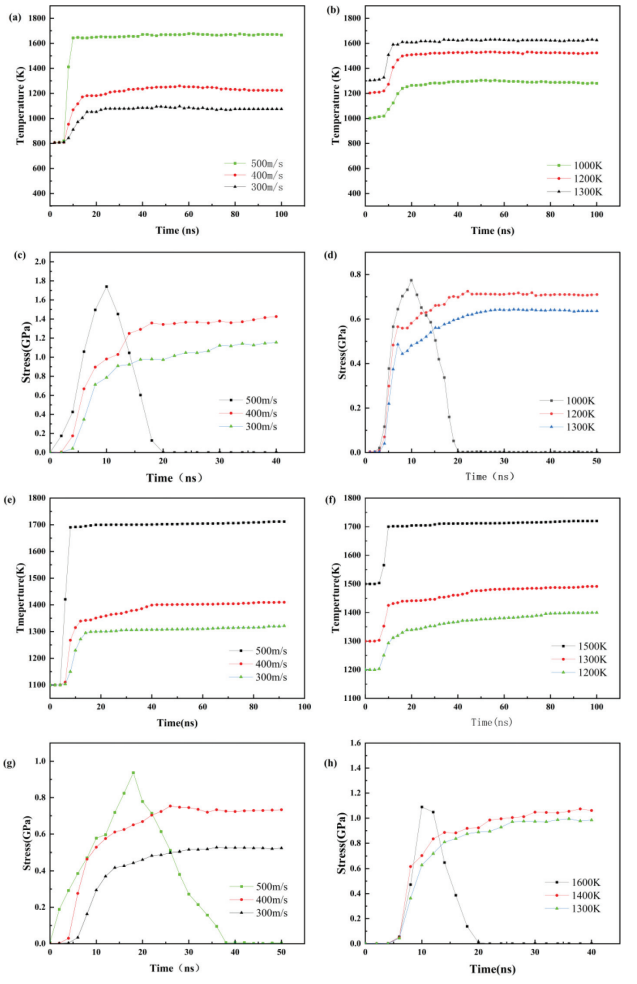

Figure 3: Comparison of heating capacities between WC-Co (a-b) particles and 316L stainless steel particles (e-f) under different temperatures and velocities. Evolutions of flow stress at the tracking nodes of WC-Co (c-d) particles and 316 stainless steel particles (g-h) under different impact velocities and temperatures.

perature of 316L stainless steel, as shown in **Figure 3c**. When 316L stainless steel reaches the melting point, the flow stress changes drastically and the adiabatic instability occurs, as shown in **Figure 3d**. By analyzing the data and comparing them with the simulation results for WC-Co from **Figure 3a**, it can be concluded that at an impact velocity of 500 m/s, the temperature rise for the 316L stainless steel particle is approximately 600 K, while the temperature rise for the WC-Co particle is roughly 800 K. Under an impact velocity of 300 m/s and a temperature of 1500 K, the 316L stainless steel particle reaches the melting point, as shown in **Figure 3c**. It is shown in **Figure 3d** that after 316L stainless steel reaches its melting point, the flow stress changes drastically, and the adiabatic instability occurs. By analyzing the data and comparing them with the simulation results for WC-Co, it can be concluded that at an impact velocity of 300 m/s, the temperature rise for the 316L stainless steel particle is approximately 200 K, while the temperature rise for the WC-Co particle is approximately 300 K.

3.2 Effects of particle temperature and particle diameter

To investigate the effects of temperature and particle diameter, three sets of simulations at temperatures of (300, 800, 1300) K and particle diameters of (20, 30, 40) μm were conducted. The variations in plastic strain and temperature over time at Tracking Node 3 of the particles under the above conditions are shown in **Figure 4**.

At both 320 m/s and 370 m/s impact velocities, the plastic strain rises with time, as shown in **Figure 4g**. At around 20 ns, it reaches final values of approximately 0.1 and 0.15, respectively, then it stabilizes. When the impact velocity reaches 420 m/s, the variation trend of plastic strain is different. Compared with the plastic strain behavior at 320 m/s and 370 m/s, the plastic strain at 420 m/s exhibits a more pronounced increase within the first 20 ns. At 30 ns, a drastic change occurs; the plastic strain continues to rise and reaches a final value of approximately 0.3. This increase in the strain may be accounted for by the transition of deformation mechanism from plastic to viscous. The variation in the particle temperature over time (**Figures 4d-4f**) resembles the variation in the plastic strain over time, but there are slight differences due to the presence of frictional and viscous dissipation. When the impact velocities are 320 m/s and 370 m/s, the temperature rise is small. In contrast, when the impact velocity reaches 420 m/s, the temperature exhibits a secondary rise, approaching the melting point of WC-Co. The same variation trend (plastic strain and temperature increase significantly with impact velocity,

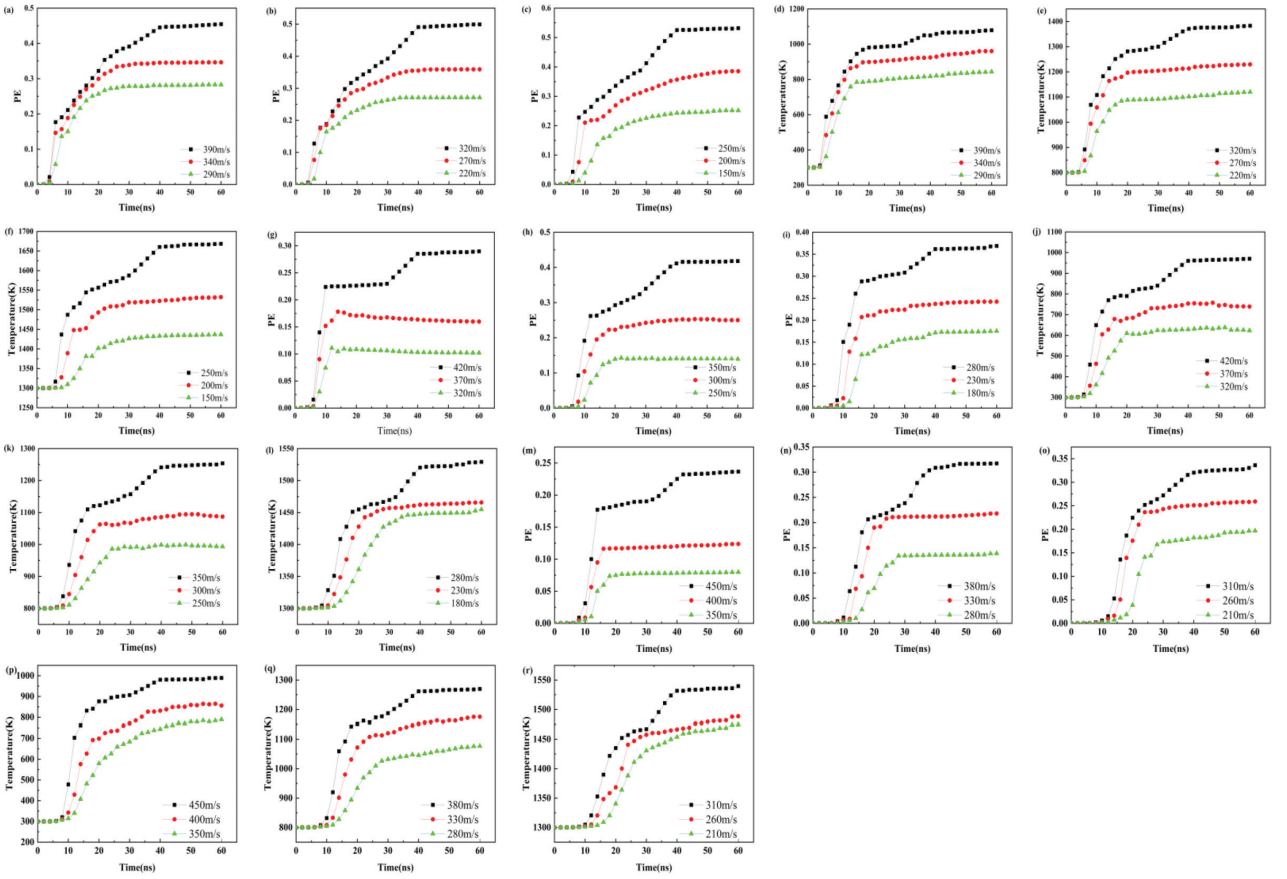

Figure 4: Plastic strain (PE) and temperature changes at different temperatures (300, 800, 1300) K of 20 μm (a–f), 30 μm (g–l), 40 μm (m–r) diameter WC-Co particles

exceeding critical value) is shown in **Figures 4a–4f** and **4m–4r**. When the velocity reaches the critical value, the temperature and plastic strain of the particle undergo a secondary rise and then tend to stabilize.

The linear relationship between critical velocity and impact temperature for particle diameters of (20, 30, and 40) μm are shown in **Figures 6a-6b**. According to these figures, particles can form an effective bond with the substrate when the impact temperature and velocity of the particles lie above the curve. As the particle diameter increases, the critical velocity required for bond formation rises accordingly. These results suggest that when large diameter particles impact the substrate, a higher impact velocity is required to achieve bonding with the substrate.

3.3 Effects of material property parameters

The above analysis reveals the temperature rise characteristics of WC-Co and 316L stainless steel. WC-Co particles, which have both high thermal conductivity and low specific heat capacity, can transfer external heat to their interior more efficiently during the temperature-rise process. Thus, this combination of properties leads to a rapid increase in the local temperature. Meanwhile, because WC-Co particles have low specific heat capacity, they absorb less heat per unit mass. During the temperature rise, the temperature change is more significant. By contrast, 316L stainless steel, which has low thermal conductivity and high specific heat capacity, has a lower heat transfer efficiency than WC-Co particles. When the local temperature of a material (e.g., 316L stainless steel) is high, its temperature changes more slowly. This is because a high specific heat capacity means that the material must absorb more heat per unit mass to change its temperature.

To investigate the two materials, numerical simulations were used to explore the variation evolutions of critical velocity varying with temperature. The comparison of the variation evolutions of the two materials and the verification of the simulation results were conducted. In Section 3.2, the numerical simulations and analysis of the variation in the critical velocity of WC-Co with temperature are presented. This section focuses on studying the relationship between the critical velocity of 316L stainless steel, the temperature and the particle diameter. The research results for 316L stainless steel are compared with the critical velocity of WC-Co varying with the temperature. The study seeks to explore the effect of the intrinsic properties of the materials on the particle deposition mechanism during impact. The variation trends of the critical velocity of 316L stainless steel with

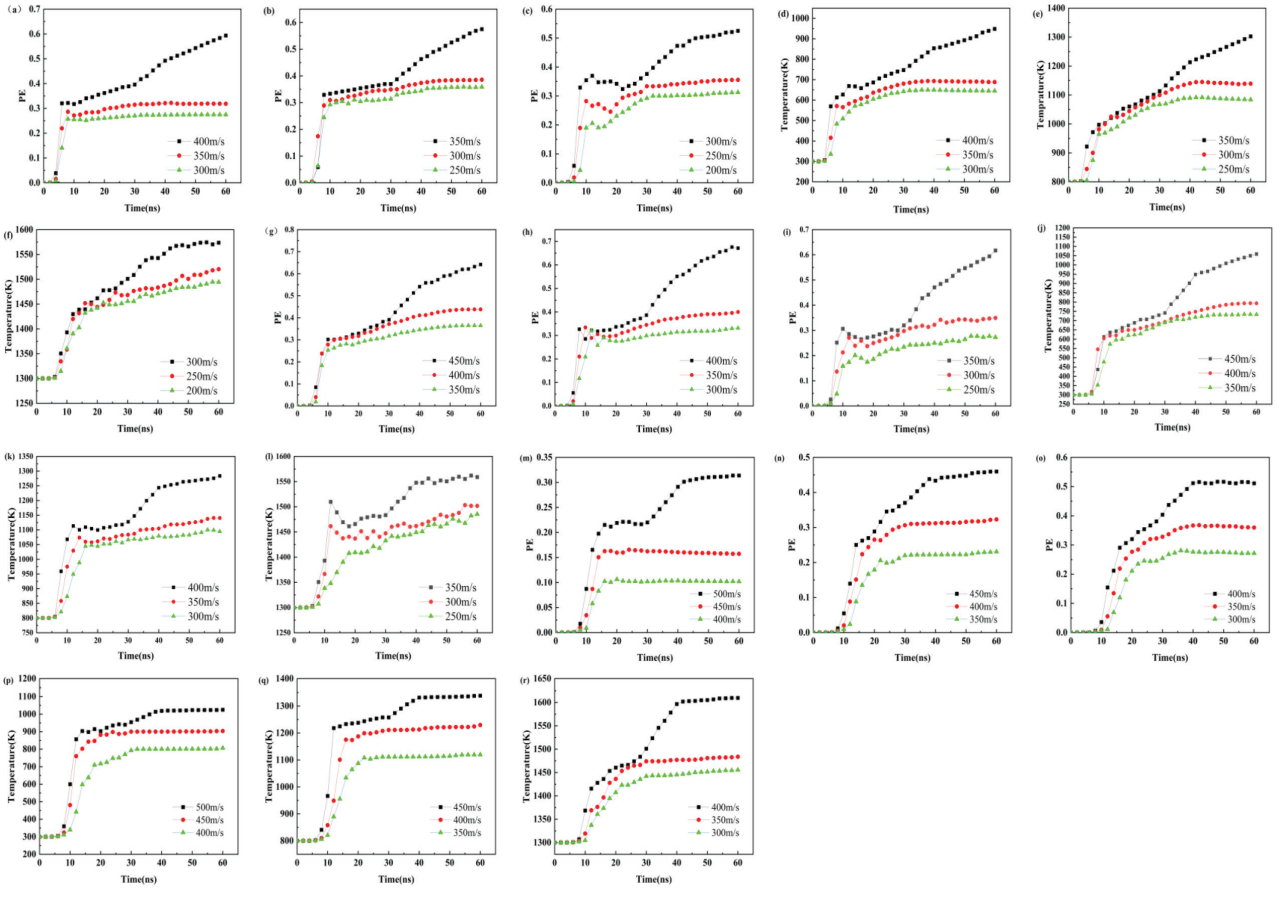

Figure 5: PE and temperature changes at different temperatures (300, 800, 1300) K of 20 μm (a–f), 30 μm (g–l), 40 μm (m–r) diameter 316L stainless steel

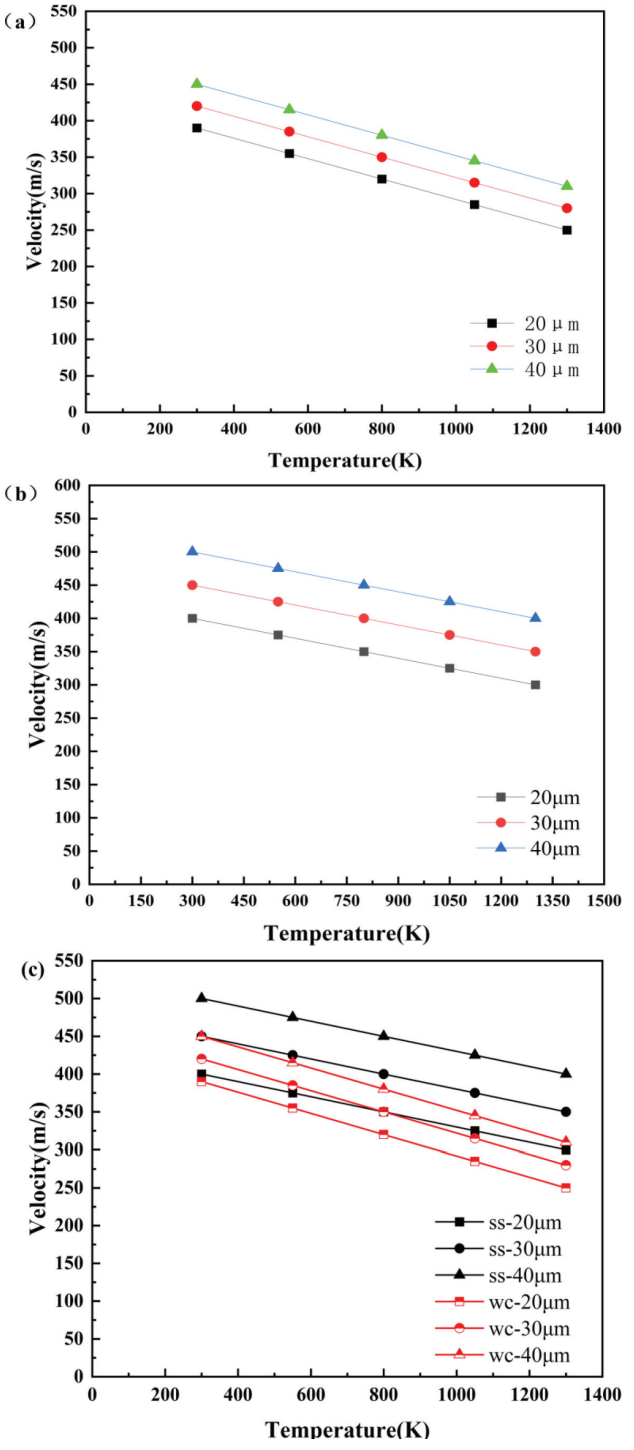

Figure 6: Variation in critical velocity with impact temperature for WC-Co: a) and 316L, b) stainless steel particles at three particle diameters (20, 30, and 40) μm, c) plot comparing the effects of temperature and particle diameter on critical velocity between 316L stainless steel and WC-Co ("ss" refers to 316L stainless steel and "wc" denotes WC-Co)

the temperature and particle diameter are illustrated in **Figure 5**.

By summarizing the above simulation results, the functional relationships between the critical velocity and impact temperature of 316L stainless steel particles with three particle diameters (20, 30, and 40) μm are obtained, as shown in **Figure 6b**.

A comparative analysis of the critical velocity variation in the two materials (WC-Co and 316L stainless steel) with particle diameter and temperature is presented in **Figure 6c**. Thus, it can be concluded that heat can be rapidly transferred within the WC-Co particles, due to their high thermal conductivity, during the heating process. Furthermore, due to the low specific heat capacity of WC-Co particles, less heat is absorbed per unit mass of the material, leading to a rapid elevation of the local temperature within the particles. The plastic strain and deposition behavior of particles undergo drastic changes, which in turn cause the critical velocity to decrease significantly. 316L stainless steel particles, with low thermal conductivity and high specific heat capacity, exhibit a low heat transfer rate. Additionally, more heat is absorbed per unit mass of this material, which in turn causes their temperature to rise slowly. The plastic strain and deposition behavior of these particles exhibit gentle changes, and the critical velocity decrease is small.

The deposition rate of the materials with high thermal conductivity and low specific heat capacity (such as WC-Co) can be improved by elevating particle temperature and significantly reducing the critical velocity. For the materials that exhibit low thermal conductivity and high specific heat capacity (such as 316L stainless steel), increasing particle velocity is more effective for enhancing the deposition rate than increasing the temperature of particles. This is because the difference in the critical velocity between high and low temperatures is small, and a significant temperature rise can only cause a minimal decrease in the critical velocity.

4 CONCLUSIONS

This study establishes a finite element (FE) model to explore the correlation between the critical velocity of HVOF thermal spray particles (WC-Co and 316L stainless steel) and two influencing parameters (temperature and particle diameter). It provides a theoretical basis for improving coating quality and optimizing spraying parameters. The conclusions based on the conducted single particle simulation are summarized as follows:

1) Particles with higher temperature exhibit lower critical velocity and are more likely to form effective bonding with the substrate. This is because higher temperatures change the physical state of particles, making them more prone to plastic deformation that facilitate bonding when they impact the substrate.

2) Particles with smaller diameters display a lower critical velocity, with a linear correlation between critical velocity and particle diameter. As the particle diameter increases, the critical velocity required for bonding with the substrate increases as well. Large-diameter particles need a higher velocity to achieve effective bonding.

3) Materials characterized by high thermal conductivity and low specific heat capacity exhibit better temperature-rise capability. The greater the temperature-rise capability, the more sensitive the material is to temperature changes, thereby more significantly affecting the critical velocity.

Acknowledgements

This work was supported by the Educational Commission of Liaoning Province of China under Grant No. LJ212410148054.

5 REFERENCES

[1] L. N. Moskowitz, Application of HVOF Thermal Spraying to Solve Corrosion Problems in the Petroleum Industry—An Industrial Note, J. Therm. Spray Technol., 2 (**1993**) 1, 21–29, doi:10.1007/bf02647419

[2] B. Wielage, A. Wank, H. Pokhmurska, T. Grund, C. Rupprecht, G. Reisel, E. Friesen, Development and trends in HVOF spraying technology, Surf. Coat. Technol., 201 (**2006**) 5, 2032–2037, doi:10.1016/j.surfcoat.2006.04.049

[3] S. Kamnis, S. Gu, 3-D modelling of kerosene-fuelled HVOF thermal spray gun, Chem. Eng. Sci., 61 (**2006**) 16, 5427–5439, doi:10.1016/j.ces.2006.04.005

[4] S. Kamnis, S. Gu, Numerical modelling of propane combustion in a high velocity oxygen–fuel thermal spray gun, Chem. Eng. Process. Process Intensif., 45 (**2006**) 4, 246–253, doi:10.1016/j.cep.2005.06.011

[5] S. Kamnis, S. Gu, T. J. Lu, C. Chen, Numerical modelling of sequential droplet impingements, J. Phys. D: Appl. Phys., 41 (**2008**) 16, 165303, doi:10.1088/0022-3727/41/16/165303

[6] S. Kamnis, S. Gu, T. J. Lu, C. Chen, Numerical modeling the bonding mechanism of HVOF sprayed particles, Comput. Mater. Sci., 46 (**2009**) 4, 1038–1043, doi:10.1016/j.commatsci.2009.05.009

[7] A. Srikanth, G. Mohammed Thalib Basha, B. Venkateshwarlu, A Brief Review on Cold Spray Coat. Process, Mater. Today: Proc., 22 (**2020**), 1390–1397

[8] G. Liang, C. J. Zhou, Y. X. Liu, Critical Velocity Prediction and Characterization of Bonding Types of High-Velocity, Air-Fuel-Sprayed Titanium Coating on Aluminum Alloys, Coatings, 12 (**2022**) 2, 234, doi:10.3390/coatings12020234

[9] A. Moridi, S. M. Hassani-Gangaraj, M. Guagliano, A hybrid approach to determine critical and erosion velocities in the cold spray process, Appl. Surf. Sci., 273 (**2013**), 617–624, doi:10.1016/j.apsusc.2013.02.089

[10] C. J. Huang, A. List, J. J. Shen, B. L. Fu, S. Yin, T. Chen, B. Klusemann, F. Gärtner, T. Klassen, Tailoring powder strengths for enhanced quality of cold sprayed Al6061 deposits, Mater. Des., 215 (**2022**), 110494, doi:10.1016/j.matdes.2022.110494

[11] A. M. Vilardell, N. Cinca, S. Dosta, I. G. Cano, J. M. Guilemany, Feasibility of using low pressure cold gas spray for the spraying of thick ceramic hydroxyapatite coatings, Int. J. Appl. Ceram. Technol., 16 (**2018**) 1, 221–229, doi:10.1111/ijac.13088

[12] L. Alonso, M. A. Garrido-Maneiro, P. Poza, A study of the parameters affecting the particle velocity in cold-spray: Theoretical results and comparison with experimental data, Addit. Manuf., 67 (**2023**), 103479, doi:10.1016/j.addma.2023.103479

[13] X. M. Wang, F. Feng, M. A. Klecka, M. D. Mordasky, J. K. Garofano, T. El-Wardany, A. Nardi, V. K. Champagne, Characterization and modeling of the bonding process in cold spray additive manufacturing, Addit. Manuf., 8 (**2015**), 149–162, doi:10.1016/j.addma.2015.03.006

[14] J. X. Yu, X. Liu, Y. Yu, Z. M. Li, S. B. Xu, H. D. Li, P. F. Liu, L. M. Wang, Effect of HVOF Spraying Process on Particle Behavior of Fe-Based Amorphous Alloy Coatings, J. Therm. Spray Technol., 31 (**2022**) 8, 2448–2462, doi:10.1007/s11666-022-01476-z

[15] H. Ruiz-Luna, D. Lozano-Mandujano, J. M. Alvarado-Orozco, A. Valarezo, C. A. Poblano-Salas, L. G. Trápaga-Martínez, F. J. Espinoza-Beltrán, J. Muñoz-Saldaña, Effect of HVOF Processing Parameters on the Properties of NiCoCrAlY Coatings by Design of Experiments, J. Therm. Spray Technol., 23 (**2014**) 6, 950–961, doi:10.1007/s11666-014-0121-2

[16] B. Sun, H. Fukanuma, N. Ohno, Study on stainless steel 316L coatings sprayed by a novel high pressure HVOF, Surf. Coat. Technol., 239 (**2014**), 58–64, doi:10.1016/j.surfcoat.2013.11.018

[17] C. Lyphout, P. Nylén, L. Östergren, Relationships Between Process Parameters, Microstructure, and Adhesion Strength of HVOF Sprayed IN718 Coatings, J. Therm. Spray Technol., 20 (**2010**) 1–2, 76–82, doi:10.1007/s11666-010-9543-7

[18] A. R. C. Nascimento, F. B. Ettouil, C. Moreau, S. Savoie, R. Schulz, Production of Babbitt Coatings by High Velocity Oxygen Fuel (HVOF) Spraying, J. Therm. Spray Technol., 26 (**2017**) 7, 1732–1740, doi:10.1007/s11666-017-0615-9

[19] W. Tillmann, S. Kuhnt, I. T. Baumann, A. Kalka, E.-C. Becker-Emden, A. Brinkhoff, Statistical Comparison of Processing Different Powder Feedstock in an HVOF Thermal Spray Process, J. Therm. Spray Technol., 31 (**2022**) 5, 1476–1489, doi:10.1007/s11666-022-01392-2

[20] C. M. Hackett. T. C. Hanson, G. S. Settles, Independent Control of HVOF Particle Velocity and Temperature, J. Therm. Spray Technol., 11 (**2002**) 1, 75–85, doi:10.1361/105996302770349005

[21] H. Assadi, F. Gärtner, T. Stoltenhoff, H. Kreye, Bonding mechanism in cold gas spraying, Acta Mater., 51 (**2003**) 15, 4379–4394, doi:10.1016/s1359-6454(03)00274-x

[22] J. M. Guilemany, V. V. Sobolev, J. C. Garmier, J. A. Calero, Modelling of particle movement and thermal behaviour during high velocity oxy-fuel spraying, Surf. Coat. Technol., 63 (**1994**) 3, 181–187, doi:10.1016/0257-8972(94)90096-5